Japanese Journal of Applied Physics

The Japan Society of Applied Physics

REGULAR PAPER • OPEN ACCESS

Numerical calculation of thermoreflectance coefficient of c-Si for wavelengths of 200–800 nm and temperatures of 300–500 K

To cite this article: Masaki Shimofuri *et al* 2023 *Jpn. J. Appl. Phys.* **62** 112006

OPEN ACCESS

Japanese Journal of Applied Physics **62**, 112006 (2023) **REGULAR PAPER**

https://doi.org/**10.35848/1347-4065/ad07f8**

Numerical calculation of thermoreflectance coefficient of c-Si for wavelengths of 200–800 nm and temperatures of 300–500 K

Masaki Shimofuri[1*], Taichi Murakami[2], Shugo Miyake[2], Amit Banerjee[1], Jun Hirotani[1], and Toshiyuki Tsuchiya[1]

[1]*Department of Microengineering, Kyoto University, Kyoto, Kyoto 615-8540, Japan*
[2]*Department of Mechanical Engineering, Kobe City College of Technology, Kobe, Hyogo 651-2194, Japan*

[*]E-mail: m_shimofuri@nms.me.kyoto-u.ac.jp

Received October 2, 2023; accepted October 30, 2023; published online November 17, 2023

In this paper, the thermoreflectance (TR) coefficient of c-Si is numerically calculated over the wavelength range of 200–800 nm and the temperature range of 300–500 K using a complex permittivity model that considers interband transitions and free carriers. The calculated results are in good agreement with literature values, and it is found that the temperature dependence of the TR coefficient is almost negligible at wavelengths above 500 nm. On the other hand, in the wavelength range of 200–500 nm, the TR coefficient depends strongly on the wavelength, and the temperature stability also changes significantly depending on the wavelength. This suggests that the wavelength of the probe light for TR measurement should be appropriately selected to realize high sensitivity and temperature stability, considering the constraints of the optical system and the temperature range of the sample. © 2023 The Author(s). Published on behalf of The Japan Society of Applied Physics by IOP Publishing Ltd

1. Introduction

The thermoreflectance (TR) is used in temperature measurement based on the temperature dependence of the reflectance of the material surface. TR measurement is a non-invasive, noncontact, high-speed, high-spatial and temperature-resolution, and high-accuracy method; therefore, it has been used especially for the measurements of the temperature and thermal properties of micro and nano materials.[1–9] In addition, the temperature mapping of gold nanowires using TR has recently been reported,[10] and TR measurement is expected to realize large-area temperature mapping with high spatial and temperature resolutions.[11,12] In current TR measurement methods, a metal film with well-known optical properties and a large reflectance change with respect to temperature change (TR coefficient) is generally deposited on the surface of a sample by vapor deposition or plating.[8,9]

However, in many cases, it is difficult to form a metallic reflective film owing to design or manufacturing process restrictions, and the importance of TR measurement for nonmetallic materials is increasing. With the improvement of the sensitivity of optical elements and the development of measurement techniques, even smaller reflectance changes can be measured with high accuracy. Recently, there have been more reports on TR measurement methods without using metal reflective films on nonmetallic materials such as silicon[13–15] and GaAs.[8,16] In particular, single-crystal silicon (c-Si) occupies a large area in MEMS and semiconductor devices, and the TR measurement of c-Si should play an important role in measuring their temperature distribution and evaluating their thermal characteristics.

In TR measurement, it is required that the reflectance itself and TR coefficient be large, and the temperature stability of the TR coefficient be high over the measurement range. Therefore, the light source for the TR measurement of c-Si should be carefully selected, taking into account the constraints of the optical system and the temperature range of samples. This requires that the reflectance and TR coefficient be clear over wide ranges of wavelengths and temperatures.

Regarding papers on the TR of c-Si, Balzarotti and Grandolfo[13] measured the TR coefficient of a c-Si sample at 300 K in the wavelength range of 200–500 nm for normal incident light and 55° oblique incident light while modulating the temperature of the sample with a 10 Hz square wave current. Furthermore, they discussed the relationship between the singularity of the TR coefficient with respect to wavelength and the band structure of Si. Shio et al.[14] numerically calculated the TR coefficient of Si at 300 K in the wavelength range of 200–500 nm. They measured the reflectance change in the temperature range of 300–500 K using a 365 nm LED light source obliquely incident at 70° and compared the measurement results with the calculation results. Heller et al.[17] measured the TR coefficients of a c-Si sample in the range of 300–500 K using a 633 and 1047 nm light source obliquely incident at 65°. A theoretical discussion of TR considering the semiconductor band structure has been summarized by Matatagui et al., but they did not cover the entire visible light region.[18] As such, measurement reports and theoretical approaches on the TR of c-Si are limited to narrow ranges of temperatures and wavelengths.[13,14,17,18]

This study is conducted to numerically calculate the TR of c-Si over wide wavelength (200–800 nm) and temperature (300–500 K) ranges, and to provide quantitative guidelines for constructing measurement systems (especially for selecting the wavelength of the probe beam) and validating experimental results.

2. Experimental methods

2.1. Complex permittivity and TR coefficient

When the temperature of a material changes, the plasma frequency and electron energy band structure change owing to the volume change, resulting in a change in the complex permittivity of the material.[19] This is often observed as a change in the reflectance of the material surface, and this relationship is

linear for many materials with any probe beam wavelengths.[13,18] TR is used to measure the temperature change of materials from the reflectance change using this relationship.

Consider the case where a laser beam, which can be regarded as a TEM00-mode Gaussian beam, is focused by a lens with negligible aberration and is incident vertically from a vacuum or air on the material surface. If the diameter of the beam waist is larger than the laser wavelength and the near-axis approximation is applicable, the incident beam can be approximated as a plane-wave light incident perpendicularly to the material surface.[20] Therefore, when the complex permittivity of the material is given by $\hat{\varepsilon} = \varepsilon_1 + i\varepsilon_2$, the observed reflectivity R can be approximated using Fresnel's equation for the normal incidence case;

$$R = \frac{(n-1)^2 + \kappa^2}{(n+1)^2 + \kappa^2}, \tag{1}$$

$$\varepsilon_1 = n^2 - \kappa^2, \tag{2}$$

$$\varepsilon_2 = 2n\kappa, \tag{3}$$

where n and κ are the refractive index and extinction coefficient of the material respectively. When ΔT increases with respect to a certain reference temperature T, the reflectance changes are as follows:

$$\frac{\Delta R}{R} \approx \frac{4(n^2 - \kappa^2 - 1)\Delta n + 8n\kappa\Delta\kappa}{[(n-1)^2 + \kappa^2][(n+1)^2 + \kappa^2]}, \tag{4}$$

where Δn and $\Delta\kappa$ are the changes in refractive index and extinction coefficient caused by the temperature change ΔT. Using α_S and β_S, which are called Seraphine coefficients that can be calculated from the relationship of $\hat{\varepsilon}$ with n and κ, we can further rewrite them with the complex permittivity change $\Delta\hat{\varepsilon} = \Delta\varepsilon_1 + i\Delta\varepsilon_2$ as follows:[8]

$$\frac{\Delta R}{R} \approx \alpha_S\Delta\varepsilon_1 + \beta_S\Delta\varepsilon_2, \tag{5}$$

$$\alpha_S = \frac{2A}{A^2 + B^2}, \tag{6}$$

$$\beta_S = \frac{2B}{A^2 + B^2}, \tag{7}$$

$$A = n(n^2 - 3\kappa^2 - 1), \tag{8}$$

$$B = \kappa(3n^2 - \kappa^2 - 1). \tag{9}$$

Therefore, once the complex permittivity and its temperature coefficient at a temperature are obtained, the TR coefficient of the material $(1/R)(\partial R/\partial T)$ is calculated.

2.2. Numerical model of complex permittivity of c-Si

The complex permittivity of c-Si can be roughly divided into the interband transition and free carrier contribution

$$\hat{\varepsilon}_{\mathrm{Si}} = \hat{\varepsilon}_{\mathrm{Si,IB}} + \hat{\varepsilon}_{\mathrm{Si,FC}}. \tag{10}$$

2.2.1. Contribution from interband transitions. The model dielectric function (MDF) model has been proposed for the contribution of interband transitions to the complex permittivity of c-Si, which takes into account the energy band structure.[21] Among parameters of the MDF model, the temperature dependence of parameters related to direct transitions was measured by Jiang et al. in the temperature range of 293–803 K and the wavelength range of 250–700 nm using p-type c-Si (the acceptor concentration was estimated as 10^{15} cm^{-3}).[22]

$$\hat{\varepsilon}^{\mathrm{direct}}_{\mathrm{Si,IB}}(\omega) = \sum_{i=1}^{6} \hat{\varepsilon}_i(\omega) \tag{11}$$

$$\hat{\varepsilon}_1(E) = -\frac{B_1 \ln(1 - X_1^2)}{X_1^2}$$

$$\hat{\varepsilon}_2(E) = \frac{B_{1X}}{E_1 - E - i\Gamma_1}$$

$$\hat{\varepsilon}_3(E) = -\frac{F \ln \frac{1-\chi_{cl}^2}{1-\chi_{2m}^2}}{\chi_{2m}^2}$$

$$\hat{\varepsilon}_4(E) = \frac{C_4 E_2^2}{E_2^2 - E^2 + i\gamma_4 E E_2}$$

$$\hat{\varepsilon}_5(E) = \frac{C_5 E_0'^2}{E_0'^2 - E^2 + i\gamma_5 E E_0'}$$

$$\hat{\varepsilon}_6(E) = \frac{C_6 E_1'^2}{E_1'^2 - E^2 + i\gamma_6 E E_1'}$$

$$X_1 = \frac{E + i\Gamma_1}{E_1}$$

$$\chi_{2m} = \frac{E + i\Gamma_2}{E_2}$$

$$\chi_{cl} = \frac{E + i\Gamma_2}{E_1}$$

$$E = h\omega.$$

Here, h is Plank constant. The temperature dependence of the parameters measured by Jiang et al. can be approximated by linear regression as follows:

$$E_1 = -4.2 \times 10^{-4}T + 3.49,$$

$$B_1 = 6.05 \times 10^{-4}T + 6.13,$$

$$\Gamma_1 = 0.076,$$

$$B_{1x} = -1.17 \times 10^{-3}T + 1.69,$$

$$E_2 = -3.2 \times 10^{-4}T + 4.3,$$

$$\Gamma_2 = -4.0 \times 10^{-5}T + 0.105,$$

$$F = -4.3 \times 10^{-3}T + 5.25,$$

$$C_4 = 2.9 \times 10^{-3}T + 1.44,$$

$$\gamma_4 = 1.4 \times 10^{-4}T + 0.0492,$$

$$E_0' = -8.5 \times 10^{-4}T + 3.49,$$

$$C_5 = 2.45 \times 10^{-4}T + 0.0194,$$

$$\gamma_5 = 2.32 \times 10^{-5}T + 0.0755,$$

$$E_1' = 5.33,$$

$$C_6 = 0.164,$$

$$\gamma_6 = 0.077.$$

Silicon is an indirect transition semiconductor, and direct transitions do not occur for lights from band-gap energy to critical energy for direct transitions (1.1–3.3 eV). However, weak absorption occurs owing to the interaction between electrons near the band edge and phonons. The parameters given by Jiang et al. do not include the contribution of the electron–phonon interaction, resulting in deviations from experimental values in wavelengths longer than 500 nm. A model for the interaction between the electrons in the band edge and phonons interaction is given by Eq. (12),[23] the temperature dependence of which has been experimentally measured by Timans[24]

$$\alpha_{\mathrm{Si,IB}}^{\mathrm{indirect}}(E, T) = \sum_{i=1}^{4}\left[\frac{F_i(E - E_g(T) + k\theta_i)}{\exp(\theta_i/T) - 1} + \frac{F_i(E - E_g(T) - k\theta_i)}{1 - \exp(-\theta_i/T)}\right] \tag{12}$$

$$F_1(x) = \begin{cases} 0.504\sqrt{x} + 392(x - 0.0055)^2 & (0.0055 \leqslant x) \\ 0.504\sqrt{x} & (0 < x < 0.0055) \\ 0 & (x \leqslant 0) \end{cases}$$

$$F_2(x) = \begin{cases} 18.08\sqrt{x} + 5760(x - 0.0055)^2 & (0.0055 \leqslant x) \\ 18.08\sqrt{x} & (0 < x < 0.0055) \\ 0 & (x \leqslant 0) \end{cases}$$

$$F_3(x) = \begin{cases} 536x^2 & (0 \leqslant x) \\ 0 & (x < 0) \end{cases}$$

$$F_4(x) = \begin{cases} 988x^2 & (0 \leqslant x) \\ 0 & (x < 0) \end{cases}$$

$$E_g(T) = 1.155 - 4.73 \times 10^{-4}\frac{T^2}{635 + T} \tag{13}$$

$$\theta_{1-4} = 212,\ 670,\ 1050,\ 1420[\mathrm{K}]. \tag{14}$$

Here, α is the absorption coefficient, which can be written as $\kappa = \alpha\lambda/4\pi$ using the extinction coefficient κ and the light wavelength λ. E_g is the band gap energy. One simple way to smoothly connect these two models at around 500 nm is to weight them using the sigmoid function w

$$\hat{\varepsilon}_{\mathrm{IB}}(\lambda) = w(\lambda)\hat{\varepsilon}_{\mathrm{IB}}^{\mathrm{direct}}(\lambda) + (1 - w(\lambda))\hat{\varepsilon}_{\mathrm{IB}}^{\mathrm{indirect}}(\lambda) \tag{15}$$

$$w(\lambda) = \frac{1}{1 + \exp\left(a\frac{\lambda_0 - \lambda}{\lambda_w}\right)}. \tag{16}$$

Here, λ_0 is the center wavelength of the connection and λ_w is the width of the connection. In this paper, λ_0 and λ_w are set to 500 and 200 nm, respectively, and a is set to 4.6 so that the effect of the smaller contribution at the edge of the connection region becomes 1%.

In actual devices, impurity-doped c-Si is often used instead of intrinsic Si, and the effect of dopant concentration must be considered. Studies on the effect of dopant concentration on the temperature dependence of interband transitions are limited to highly doped cases (N_D, $N_A > 10^{19}$ cm^{-3}) and no data are available for lightly doped c-Si (N_D, $N_A \approx 10^{17}$ cm^{-3}). Heavy doping is known to affect interband transitions[25–27] (see Fig. 1 in Sect. 3). On the other hand, according to Basta's model,[28] the effect of dopant concentration on interband transitions is negligible in lightly doped c-Si (N_D, $N_A \approx 10^{17}$ cm^{-3}). Therefore, the effect of impurity concentration on interband transitions is not considered in this paper.

2.2.2. Contribution of free carriers. Most of the lasers for TR measurements use visible light, and in this wavelength region, interband transitions predominate, and the effect of free carriers has been considered negligible. However, in semiconductors, the free carrier concentration changes rapidly with temperature, and its effect on the TR coefficient

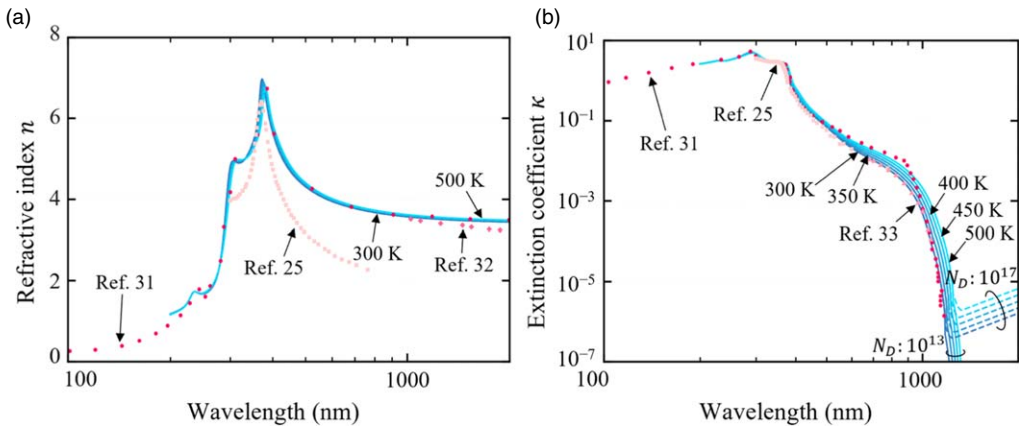

Fig. 1. Calculated (a) refractive index and (b) extinction coefficient of c-Si. The blue solid and dashed curves are respectively the calculated results for intrinsic and doped ($N_D = 10^{13}$, 10^{17} cm^{-3}) c-Si at 300, 350, 400, 450, and 500 K. Red circles, squares, diamonds, and triangles are experimentally measured values from Refs. 25 ($N_D = 9 \times 10^{18}$ cm^{-3}),[31] (intrinsic),[32] ($N_D = 1 \times 10^{20}$ cm^{-3}), and[33] (intrinsic), respectively.

may not be negligible. Therefore, it is considered in the calculations.

The contribution of the free carriers of c-Si to the complex permittivity can be expressed using the Drude model as follows[23]:

$$\hat{\varepsilon}_{\mathrm{Si,FC}}(\omega) = -\frac{e^2}{\varepsilon_0}\left(\frac{N_e}{m_e^*}\frac{1}{\omega + \frac{i\omega}{\tau_e}} + \frac{N_h}{m_h^*}\frac{1}{\omega + \frac{i\omega}{\tau_h}}\right), \tag{17}$$

where e is the elementary charge, $N_{e,h}$ is the electron and hole concentrations, and $m_{e,h}^*$ is the effective mass of electrons and holes. In the case of metals, the concentration of free carriers is constant regardless of temperature because the Fermi level exists in the conduction band above RT, and only τ_e depends on temperature. On the other hand, in the case of semiconductors, since the Fermi level exists in the band gap, the temperature-dependent parameters include not only $\tau_{e,h}$ but also $N_{e,h}$. The temperature dependence of $\tau_{e,h}$ in the case of silicon is given by the following equation:[23]

$$\frac{1}{\tau_{e,h}} = \frac{1}{\tau_{e,h-l}} + \frac{1}{\tau_{e,h-d}}, \tag{18}$$

$$\tau_e^0 = \frac{195}{1 + \left(\frac{N_D}{1.3 \times 10^{17}[\mathrm{cm}^{-3}]}\right)^{0.91}} + 14.1,$$

$$\tau_h^0 = \frac{94}{1 + \left(\frac{N_A}{1.9 \times 10^{17}[\mathrm{cm}^{-3}]}\right)^{0.76}} + 10,$$

$$\tau_{e-l}^0 = 2.23 \times 10^2,$$

$$\tau_{h-l}^0 = 1.06 \times 10^2,$$

$$\frac{\tau_{e-d}}{\tau_{e-d}^0} = \frac{\tau_{h-d}}{\tau_{h-d}^0} = \left(\frac{T}{300}\right)^{1.5},$$

$$\tau_{e-l} = \tau_{e-l}^0\left(\frac{T}{300}\right)^{-3.8},$$

$$\tau_{h-l} = \tau_{h-l}^0\left(\frac{T}{300}\right)^{-3.6}.$$

The free carrier concentration $N_{e,h}$ can be obtained by the charge neutrality condition (19), the impurity ionization Eqs. (20a) and (20b), and the mass action law (22) in conjunction.[29,30]

$$N_e + N_A^- = N_h + N_D^+ \tag{19}$$

$$N_D^+ = \frac{N_D}{1 + 2\exp\left[(E_F - E_D)/k_\mathrm{B}T\right]} \tag{20a}$$

$$N_A^- = \frac{N_D}{1 + 4\exp\left[(E_A - E_F)/k_\mathrm{B}T\right]} \tag{20b}$$

$$N_e = N_C \exp\left(-\frac{E_C - E_F}{k_\mathrm{B}T}\right) \tag{21a}$$

$$N_h = N_V \exp\left(-\frac{E_V - E_F}{k_\mathrm{B}T}\right) \tag{21b}$$

$$N_e N_h = N_C N_V \exp\left(-\frac{E_g}{k_\mathrm{B}T}\right) \tag{22}$$

Here, N_D and N_A are the concentrations of dopants and acceptors respectively, and superscripts indicate their ions. E_D and E_A are the energy levels of dopants and acceptors, and E_C and E_V are the energy levels at the conduction band and VB edges, respectively.

3. Calculation results and discussion

3.1. Calculation results of optical properties

The results of the calculation of n and κ of intrinsic and doped ($N_D = 10^{13}$, 10^{17} cm^{-3}) c-Si at 300, 350, 400, 450, and 500 K are shown in Fig. 1. The values obtained using the model are in good agreement with experimental values[31–33] over the entire wavelength range of the calculation. The dopant concentration has almost no effect on the temperature dependence in the visible light wavelength region (N_D, $N_A \leqslant 10^{17}$ cm^{-3}). The literature values[25] for heavily doped c-Si deviate significantly from the value obtained using the model; indicating that therefore this means the model proposed in this paper may not be applicable for heavily doped c-Si (N_D, $N_A \gg 10^{17}$ cm^{-3}).

3.2. TR coefficient calculation results

The TR coefficient is defined as[8]

$$C_{TR} = \frac{1}{R}\frac{\partial R}{\partial T}. \tag{23}$$

The calculated reflectance and TR coefficients at 300, 350, 400, 450, and 500 K are calculated using Eq. (1) shown in Fig. 2. The results are only for $N_D = 10^{13}$ cm^{-3} because the effect of impurity concentration was confirmed to be negligible for lightly doped c-Si in Sect. 3.1. Figure 2(a) shows that the reflectance has the same trend at a high temperature of about 500 K as at 300 K. c-Si has high reflectance below 400 nm, where direct transitions begin to occur, and wavelengths in this region are advantageous for TR measurements. Since reflectance decreases monotonically in the region above 400 nm, shorter wavelengths are advantageous for TR measurements.

The red dots in Fig. 2(b) are the values measured by Balzarotti and Grandolfo at 300 K,[13] and the trends are in good agreement with the calculated values; this indicates that the model is suitable for calculating the TR coefficient. There is a difference in absolute value, because the Balzarotti and Grandolfo's measurements did not consider the effects of the surface oxide or adsorption layer and the surface roughness of the sample. Jiang et al.[22] confirmed that the surface adsorption layer causes deviation from the model, and Jellison et al.[27] reported that the measured reflectance is small owing to the surface roughness of silicon. However, since these sample surface conditions have little effect on the trend of the TR coefficient, as shown in their reports,[22,27] the model proposed in this paper without these effects is sufficient for qualitative discussion.

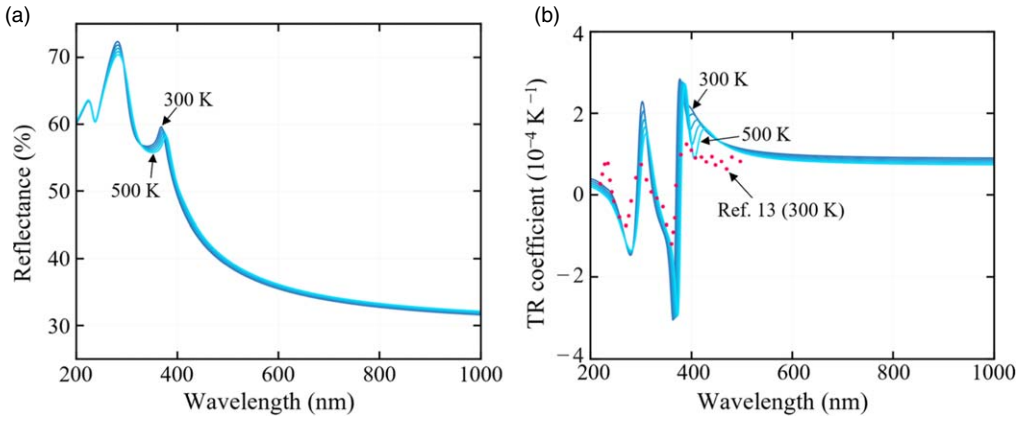

Fig. 2. (a) Reflectance of c-Si calculated for intrinsic c-Si at 300, 350, 400, 450, and 500 K; b) calculated TR coefficient (10^{-4} K^{-1}) of c-Si at 200–1000 nm at 300, 350, 400, 450, and 500 K. Red dots indicate the data obtained from Ref. 13.

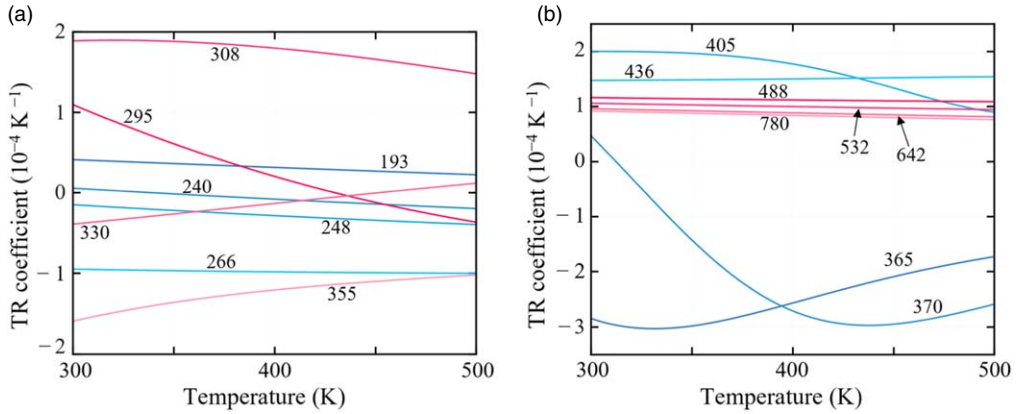

Fig. 3. (a) Temperature dependence of TR (10^{-4} K^{-1}) at 193, 240, 248, 266, 295, 308, 330, and 355 nm between 300 and 500 K; (b) temperature dependence of TR (10^{-4} K^{-1}) at 365, 370, 405, 436, 488, 532, 642, and 780 nm between 300 and 500 K.

Figure 2(b) shows that the TR coefficient decreases gradually and monotonically at wavelengths longer than 500 nm, and it is almost constant, especially at wavelengths longer than 750 nm. Therefore, compared with wavelengths longer than 500 nm, shorter wavelengths have larger TR coefficient and reflectance, which is advantageous for TR measurements. On the other hand, the TR coefficient shows a complex behavior at wavelengths shorter than 500 nm. In particular, there are singularities of TR coefficient at around 240, 295, 330, 370, and 400 nm (5.17, 4.28, 3.76, 3.35, and 3.1 eV, respectively). As pointed out by Balzarotti and Grandolfo,[13] these singularities correspond to critical points of interband transitions (3.1 eV: $L_{3'} \rightarrow L_1$, 3.4 eV: $\Gamma_{25'} \rightarrow \Gamma_{15}$, 3.8 eV: $\Gamma_{25'} \rightarrow \Gamma_{2'}$, 4.0 eV: $X_4 \rightarrow X_1$, and 5.4 eV: $L_{3'} \rightarrow L_3$[34]). The TR coefficient corresponds approximately to the wavelength derivative of permittivity, which is attributed to the shift of the absorption center wavelength due to temperature changes.[8] Therefore, these singularities can be interpreted as a strong effect of the temperature dependence of the band structure.

Figure 2(b) shows that the temperature dependence is strong at wavelengths where the curves are spread out on the vertical axis. Although the TR coefficient reaches its absolute maximum near 360 and 380 nm, its temperature dependence is significantly large, indicating that the linearity of the TR coefficient is poor. It is expected that the error will become larger for measured samples with large temperature variations or temperature distributions. The wavelengths with large TR coefficients and weak temperature dependence in the range of 300–500 K are 270 nm (TR coefficient: $-1.15 \times 10^{-4} \pm 1\%$ K^{-1}), 285 nm ($-1.2 \times 10^{-4} \pm 3\%$ K^{-1}), 310 nm ($1.6 \times 10^{-4} \pm 6\%$ K^{-1}), and 435 nm ($1.5 \times 10^{-4} \pm 1\%$ K^{-1}). These wavelengths are recommended for samples with large temperature variations or temperature distributions.

Next, the temperature dependence of the TR coefficient at 193 (ArF), 240, 248 (KrF), 266 (FHG-YAG), 295, 308 (XeCl), 330, 355 (THG-YAG), 365 (Hg: i-line), 370, 405 (Hg: g-line), 436 (Hg: h-line), 488 (InGaN), 532 (SHG-YAG), 642 (AlGaInP), and 780 nm (AlGaAs) as representative wavelengths is shown in Fig. 3. These wavelengths are frequently used optically or have positive–negative inverted TR coefficients.

From Fig. 3, it is confirmed that the TR coefficients at 266, 436, 488, 532, 642, and 780 nm are large (around 1×10^{-4} K^{-1}) and highly linear, as expected from Fig. 2(b). They are good choices for measuring samples with large temperature variations or temperature distributions. Although the wavelengths of 308, 365, 370, and 405 nm seem to be unsuitable for TR measurements owing to their low linearity as shown in Fig. 2(b), the curves at 308, 365, 370, and 405 nm take extreme values at 300, 325, 430, and 300 K, respectively. Therefore, the probe beams with these wavelengths have high sensitivity and good linearity for measurements in a narrow

temperature range around the temperatures at which the extreme values are taken. On the other hand, 193, 240, and 248 nm have poor linearity and small TR coefficients, making them unsuitable for TR measurements. 295, 330, and 355 nm have large coefficients but low linearity, so they are also unsuitable for TR measurements.

4. Conclusion

In this paper, we propose a calculation model for the TR coefficient of c-Si over wide ranges of wavelengths and temperatures, which can be used as a quantitative guideline for the construction of TR measurement systems and for the validation of experimental results.

A complex permittivity model that considers the temperature dependence of interband transitions and free carriers of c-Si was proposed and used to calculate TR coefficients in the wavelength range of 200–800 nm and the temperature range of 300–500 K. The values obtained using the proposed complex permittivity model were in good agreement with literature values for c-Si, and the calculated TR coefficients were also in good agreement with measured values. The calculations show that 308 and 405 nm can be used for probe beams in TR measurements with high sensitivity (around 2×10^{-4} K^{-1}) and good linearity at around 300 K. Similarly, 365 and 370 nm have high sensitivity (-3×10^{-4} K^{-1}) and good linearity at around 325 and 430 K, respectively. The wavelengths of 266, 436, and 488 nm have good linearity in the 300–500 K range and a large TR coefficient of $\sim 1 \times 10^{-4}$ K^{-1} (a negative coefficient at 266 nm), making them effective for probe beams for measuring samples with large temperature variations or temperature distributions. The wavelengths above 500 nm for probe beams have similar characteristics to each other, and they also have good linearity in the range of 300–500 K and a large TR coefficient of $\sim 1 \times 10^{-4}$ K^{-1}. These results should be useful in the implementation and interpretation of the conventional empirical TR measurement of c-Si.

Acknowledgments

This research was carried out with the support of JSPS KAKENHI Grant No. JP21H01261, the Yazaki Memorial Foundation for Science and Technology, and the Mori Manufacturing Research and Technology Foundation.

1) D. G. Cahill, Rev. Sci. Instrum. **75**, 5119 (2004).
2) J. Zhu, D. Tang, W. Wang, J. Liu, K. W. Holub, and R. Yang, J. Appl. Phys. **108**, 094315 (2010).
3) A. J. Schmidt, R. Cheaito, and M. Chiesa, J. Appl. Phys. **107**, 024908 (2010).
4) R. Garrelts, A. Marconnet, and X. Xu, Nanoscale Microscale Thermophys. Eng. **19**, 245 (2015).
5) J. Jeong, X. H. Meng, A. K. Rockwell, S. R. Bank, W. P. Hsieh, J. F. Lin, and Y. G. Wang, Nanoscale Microscale Thermophys. Eng. **23**, 211 (2019).
6) M. S. B. Hoque et al., ACS Nano **15**, 9588 (2021).
7) M. S. B. Hoque et al., Rev. Sci. Instrum. **92**, 064906 (2021).
8) D. Pierścińska, J. Phys. D: Appl. Phys. **51**, 013001 (2018).
9) C. Yuan, R. Hanus, and S. Graham, J. Appl. Phys. **132**, 220701 (2022).
10) K. Ridier, A. Bas, Y. Zhang, L. Routaboul, L. Salmon, G. Molnár, C. Bergaud, and A. Bousseksou, Nat. Commun. **11**, 3611 (2020).
11) J. Christofferson and A. Shakouri, Rev. Sci. Instrum. **76**, 024903 (2005).
12) G. Tessier, S. Hole, and D. Fournier, Appl. Phys. Lett. **78**, 2267 (2001).
13) A. Balzarotti and M. Grandolfo, Solid State Commun. **6**, 815 (1968).
14) K. Shio, H. Wakai, K. Kubota, and H. Akiba, Komatsu Tech. Rep. Vol. 54, No. 161, 2008, https://www.komatsu.jp/ja/aboutus/innovation/technology/techreport.
15) S. Miyake, T. Kato, H. Taguchi, and T. Namazu, Jpn. J. Appl. Phys. **55**, 06GP08 (2016).
16) N. Poopakdee, Z. Abdallah, J. W. Pomeroy, and M. Kuball, ACS Appl. Electron. Mater. **4**, 1558 (2022).
17) J. Heller, J. W. Bartha, C. C. Poon, and A. C. Tam, Appl. Phys. Lett. **75**, 43 (1999).
18) E. Matatagui, A. G. Thompson, and M. Cardona, Phys. Rev. **176**, 950 (1968).
19) R. Rosei and D. W. Lynch, Phys. Rev. B **5**, 3883 (1972).
20) P. Vaveliuk, B. Ruiz, and A. Lencina, Opt. Lett. **32**, 927 (2007).
21) S. Adachi, Phys. Rev. B **38**, 12966 (1988).
22) Z. Jiang, T. Yamaguchi, M. Aoyama, and T. Hayashi, Jpn. J. Appl. Phys. **37**, 479 (1998).
23) C. J. Fu and Z. M. Zhang, Int. J. Heat Mass Transfer **49**, 1703 (2006).
24) P. J. Timans, J. Appl. Phys. **74**, 6353 (1993).
25) G. E. Jellison Jr, Opt. Mater. **1**, 41 (1992).
26) G. E. Jellison Jr, M. F. Chisholm, and S. M. Gorbatkin, Appl. Phys. Lett. **62**, 3348 (1993).
27) G. E. Jellison Jr, S. P. Withrow, J. W. McCamy, J. D. Budai, D. Lubben, and M. J. Godbole, Phys. Rev. B: Condens. Matter **52**, 14607 (1995).
28) M. Basta and Z. T. Kuznicki, Photonics for Solar Energy Systems III7725SPIE Photonics Europe (Brussels, Belgium), 18 May (2010) p. 77251J.
29) S. M. Sze, N. K. Kwok, and L. Yiming, *Physics of Semiconductor Devices* (Wiley, New York, 2021) 4th ed.
30) K. Seeger, *Semiconductor Physics* (Springer, Berlin, Heidelberg, 2004) 9th ed.
31) E. D. Palik, *Handbook of Optical Constants of Solids* (Academic, Boston, 1985) 1st ed.
32) E. Barta, Infrared Phys. **17**, 319 (1977).
33) P. E. Schmid, Phys. Rev. B **23**, 5531 (1981).
34) E. O. Kane, Phys. Rev. **146**, 558 (1966).